Chapter 4

Synthesis of 3-aminopropyltrimethoxysilane functionalized Au/Ag bimetallic nanoparticles incorporated hydroxyapatite bioceramic and their mechanical, antibacterial as well as cellular responses

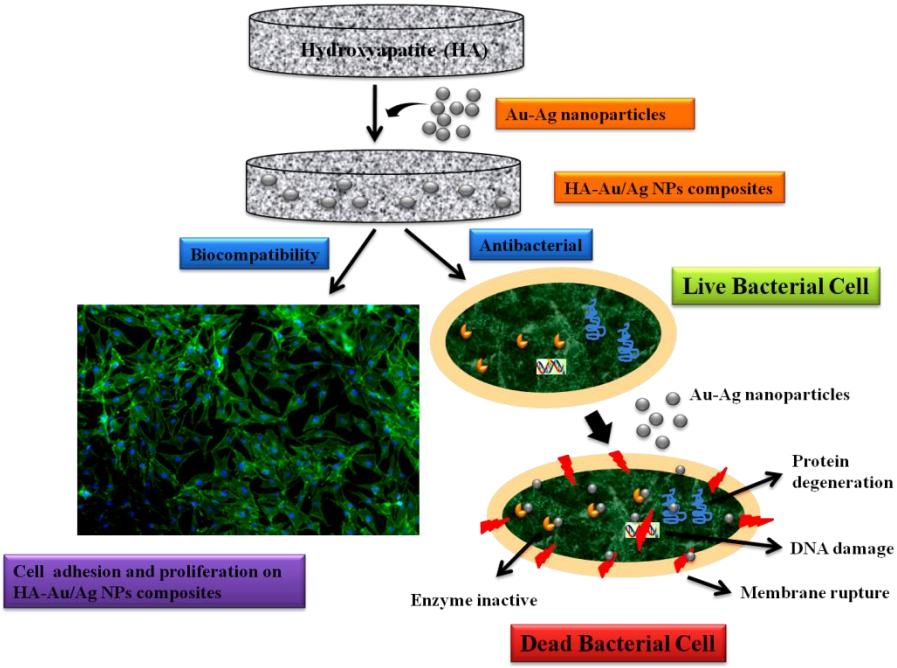

4.1 Introduction

For several years, researchers have sought biomaterials to replace human bone that exhibit appropriate mechanical attributes as well as antibacterial properties and

cytocompatibility. A bone graft is commonly used to treat bone loss due to trauma or disease (Kokubo et al., 2003). Grafts are essential to help with bone regeneration after bone loss due to bone tumor excision, accidents that cause bone loss, and bone fractures that cannot mend on their own. Over the past three decades, numerous types of bioactive ceramics such as Bioglass® (the Na_2O-CaO-SiO_2-P_2O_5 system), hydroxyapatite (HA) [$Ca_{10}(PO_4)_6(OH)_2$], tricalcium phosphate (TCP) [$Ca_3(PO_4)_2$], HA/TCP bi-phase ceramic, and glass ceramic have been used in clinical applications (Miyata et al., 2002; Kim et al., 2000). Among these bioactive ceramic materials, HA has been widely used in clinical applications (Feng et al., 2014). The size, shape, and crystal structure of HA materials has an impact on the biological properties of osteoblast cells (Haider et al., 2017). It should also be noted that crystalline inorganic material found in bone is similar to HA (Khajuria et al., 2015; Okada et al., 2015). Given that the inorganic material in bone and teeth is similar to HA. HA is considered as a scaffold material for bone tissue engineering (Radha et al., 2023; Kumar et al., 2022). However, HA exhibits inadequate fracture properties for load-bearing applications. Research efforts have focused on methods to improve the fracture resistance of HA (Zhou et al., 2011). Nanoscale structures containing HA may offer improved fracture resistance; for example, gold-silver nanoparticles (Au/Ag NPs) have been used with hydroxyapatite to create orthopaedic implants (Zhang et al., 2016; Gong et al., 2015). Chen et al. described the use of CNT-reinforced hydroxyapatite composite materials for use as coatings on load-bearing metal implants (Chen et al., 2005). Tsui et al. described the use of plasma spraying to deposit HA coatings on Ti–6Al–4V substrates; they noted that adjusting the plasma spraying parameters does not provide reasonable control over the crystallinity of the coatings (Tsui et al., 1998). Li et al. reported that adding titania (10 and 20 vol. %) as

a reinforcement to HA improved the stiffness and fracture toughness of the composite coatings (Li et al., 2002).

Silver has received significant attention from the biomaterials community due to its antimicrobial properties (Zhang et al., 2017; Victor et al., 2015). Several studies have considered using silver and gold nanoparticles for bone regeneration applications (Ribeiro et al., 2017; Heo et al., 2014; Geng et al., 2017). The functionalization of nanoparticles is also a significant focus of biomaterials research (Glenske et al., 2018). Qin et al. noted that Ag nanoparticles had been found to support osteogenic differentiation in stem cells obtained from urine (Qin et al., 2014). In another study, Ag nanoparticles significantly increased the proliferation and mineralization of MC3T3-E1 cells (Mahmood et al., 2011). Qing et al. showed using RNA-seq technology that Ag nanoparticles influence the differentiation and metabolism of MC3T3-E1 cells (Qing et al., 2018). Hsu et al. 2007 demonstrated that chondrocytes exposed to nanocomposites containing porcine type II collagen and up to 2.5 weight percent Au nanoparticles exhibited neither a change in gene expression nor cytotoxicity. Liu et al. indicated that Au nanoparticles modified the differentiation, mineralization, and proliferation of MC3T3-E1 cells in a dose-dependent manner; the expression of genes associated with alkaline phosphatase (ALP), bone morphogenetic protein 2 (BMP-2), osteocalcin (OCN), and runt-related transcription factor 2 (Runx2) increased after exposure to 20 nm and 40 nm diameter Ag nanoparticles (Heo et al., 2014; Liu et al., 2010). It should be noted that HA exhibits limitations related to its use for bone regenerative medicine applications due to its lack of mechanical and antibacterial capabilities (Gao et al., 2016). In addition, HA demonstrates agglomeration and a paucity of interfacial bonding between the polymeric matrix and the inorganic filler (Alvarez et al., 1999; Bala et al., 2006). To overcome this

problem, coupling agents have been used that modify the surface properties of the HA and thereby improve the interfacial interaction (Vaz et al., 2002). Many researchers have demonstrated the use of silanes to modify the surface characteristics of HA (Tham et al., 2010; Dupraz et al., 1996; Domingo et al., 2006; Cisneros-Pineda et al., 2014). However, previous studies have not examined the biocompatibility of these materials. Functionalization of Ag/Au nanoparticles with 3-APTMS improves their stability by providing a protective layer and preventing aggregation. The amino groups present in 3-APTMS act as stabilizing agents, forming strong covalent bonds with metal surfaces and reducing the tendency for nanoparticles agglomeration (Pandey et al., 2015). This stability ensures the long-term performance of Ag/Au nanoparticles in biomedical applications. Ag/Au nanoparticles functionalized with 3-APTMS also exhibit excellent biocompatibility and enhanced antibacterial properties. The functionalized nanoparticles can inhibit the growth of various pathogenic bacteria, including drug-resistant strains (Rai et al., 2016). The presence of amino groups on the nanoparticles surface facilitates interaction with bacterial cell membranes, leading to cell membrane disruption, oxidative stress, and subsequent bacterial death (Gopinath et al., 2017). Moreover, the hydroxyapatite matrix provides a favourable environment for cell adhesion, proliferation, and differentiation (Kobayashi et al., 2019). The combination of 3-APTMS functionalized Ag/Au nanoparticles with hydroxyapatite holds great potential for bone tissue engineering and regeneration (Wang et al., 2011; Rehman et al., 2016; Ji et al., 2023). The antibacterial properties of Ag/Au nanoparticles help prevent infection at the implant site, promoting successful integration and healing (Jiao et al., 2021). Additionally, the hydroxyapatite component mimics the natural bone mineral, providing a scaffold for cell attachment and growth. The functionalized nanoparticles can also

promote osteogenesis by stimulating bone cell differentiation and mineralization (Abdul et al., 2021). Functionalized Ag/Au nanoparticles with 3-APTMS and hydroxyapatite can be utilized as carriers for controlled drug delivery (Cintra et al., 2022; Wang et al., 2020; Mondal et al., 2019). The unique surface chemistry and high surface area of the nanoparticles enable efficient loading and release of therapeutic agents (Yetisgin et al., 2020). The sustained release of drugs from the nanoparticles surface can enhance their efficacy and reduce potential side effects (Chandrakala et al., 2022). Moreover, the antibacterial properties of the nanoparticles can help prevent infections in localized drug delivery systems. Thus, the functionalization of Ag/Au nanoparticles with 3-APTMS and their incorporation into a hydroxyapatite matrix provides numerous advantages, including enhanced stability, biocompatibility, antibacterial activity, and potential applications in bone tissue engineering and drug delivery systems. Therefore, this chapter describes the incorporation of Au/Ag NPs in HA and the mechanical properties (e.g., fracture toughness, hardness, compressive strength, and flexural strength), microstructure, and elemental composition of these materials. The antibacterial functionality of the materials was studied using gram-positive (*S. aureus*) and gram-negative (*E. coli*) bacteria. Qualitative and quantitative assays were performed to understand the antibacterial behavior of HA and HA-x Au/Ag NPs. In addition to mechanical and antibacterial testing, the present chapter also examined the cytocompatibility of sintered composites.

4.2 Results and discussion

The synthesized Au/Ag NPs were characterized using UV-Vis spectroscopy and transmission electron microscopy (TEM). The phase evolution, microstructure analysis,

thermogravimetric analysis (TGA), mechanical characterization, antibacterial, and cytocompatibility results are described in subsequent sections.

4.2.1 UV-vis spectroscopy and transmission electron microscopy (TEM)

Figure 4.1(a) contains a TEM image of the Au/Ag NPs; a higher magnification image of the Au/Ag NPs is shown in Figure 4.1(b). SAED pattern from the Au/Ag NPs is shown in Figure 4.1(c). Figure 4.1(d) shows a UV-Vis spectrum of the Au/Ag NPs. The appearance of two absorption peaks at approximately 400 nm for silver nanoparticles and 520 nm for gold nanoparticles confirmed the formation of bimetallic nanoparticles.

The formation of bimetallic Au/Ag NPs is implied by a noticeable contrast difference between lighter and darker regions in TEM image. The TEM image displayed in Figure 4.1 (b) showcases the silver-gold bimetallic nanoparticles, revealing d values of approximately 0.20 nm, which corresponds to the (200) plane of silver, and 0.23 nm, corresponding to the (111) plane of gold. These observations serve as confirmation of the formation of Au/Ag bimetallic nanoparticles.

4.2.2 Densification, phase Evolution and microstructural Analysis

The density of all of the sintered samples was measured using Archimedes's principle. After sintering, monolithic HA and HA – 2 Au/Ag NPs, HA – 5 Au/Ag NPs, and HA – 10 Au/Ag NPs composite samples exhibited approximately 95.0 ± 0.4, 96.0 ± 0.2, 97.0 ± 0.2 and 98.2 ± 0.3% densification (Figure 4.2).

The formation of pure phase HA and HA-x Au/Ag NPs was confirmed by XRD and is shown in Figure 4.3 XRD peaks at 2θ =25.96º, 29.1º, 31.88º, 32.98º, 34.1º, 39.84º, 42.2º, 43.88º, 46.74º, 48.38º, 49.54º, 50.56º, 51.42º, 52.12º, 53.26º, 61.78º, 63.22º and 65.3º are characteristic of HA (JCPDS 09-0432 card) (Verma et al., 2019).

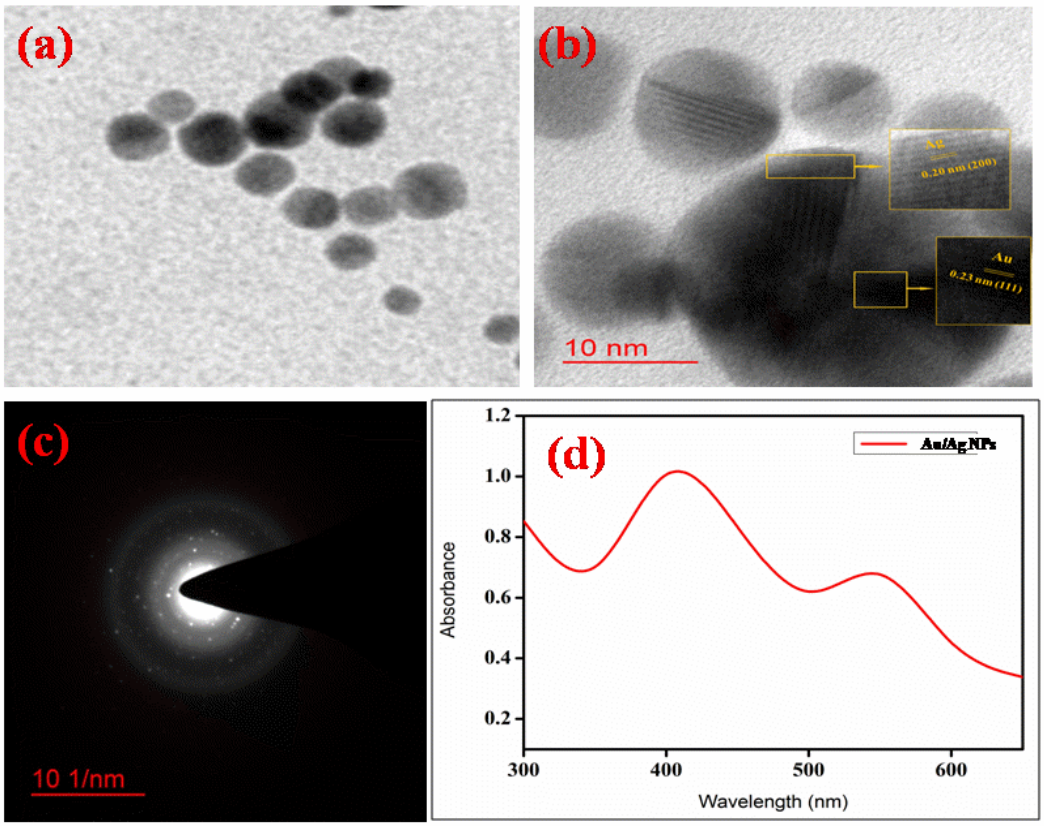

Figure 4.1 *TEM image at two different magnifications (a,b), SAED pattern (c), and UV spectra (d) of Au/Ag NPs.*

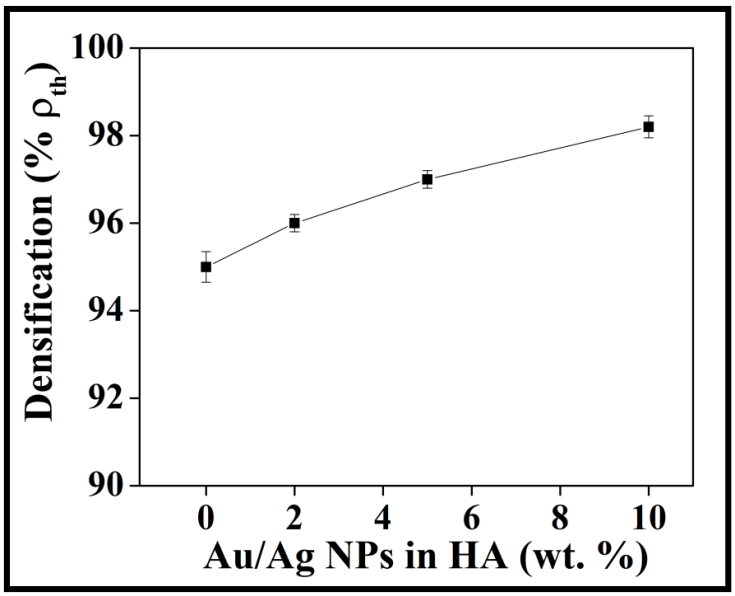

Figure 4.2 *Densification behavior of HA, HA – 2 Au/Ag NPs, HA – 5 Au/Ag NPs, and HA – 10 Au/Ag NPs composite samples.*

The formation of pure phase HA and HA-x Au/Ag NPs was confirmed by XRD and is shown in Figure 4.3 XRD peaks at 2θ =25.96º, 29.1º, 31.88º, 32.98º, 34.1º, 39.84º, 42.2º, 43.88º, 46.74º, 48.38º, 49.54º, 50.56º, 51.42º, 52.12º, 53.26º, 61.78º, 63.22º and 65.3º are characteristic of HA (JCPDS 09-0432 card) (Verma et al., 2019).

The XRD pattern of HA-x Au/Ag NPs exhibits a few additional peaks at 38.82º, 45.44º, and 64.06 associated with Au NPs and a single peak at 38.82º for Ag NPs. It is clearly observed that the XRD diffraction peaks of HA-x Au/Ag NPs are similar to those of pristine HA, which suggests that the incorporation of Au/Ag NPs is not changing the crystalline structure of HA (Liu et al., 2010).

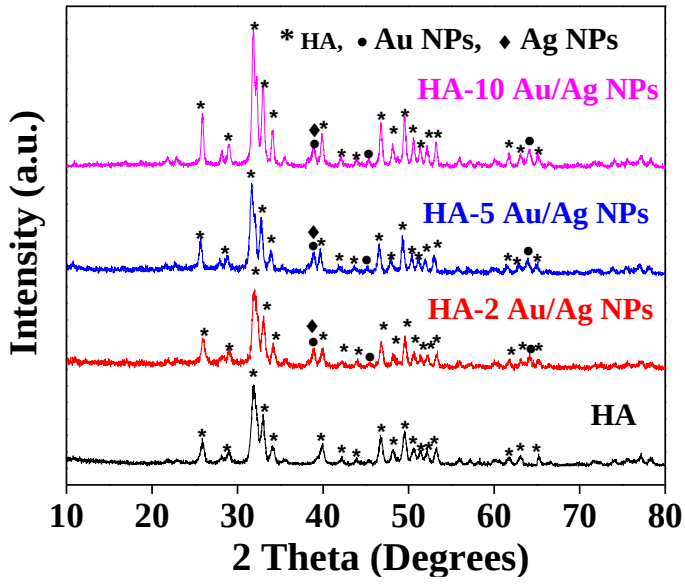

Figure 4.3 *X-ray diffraction (XRD) patterns of HA-x Au/Ag NPs (x = 0, 2, 5 and 10 wt. %) sintered samples.*

Figure 4.4 shows the SEM images of the fractured surfaces of sintered HA, HA-2 Au/Ag NPs, HA-5 Au/Ag NPs, and HA-10 Au/Ag NPs composites. It is seen in Figure 4.4 that the addition of Au/Ag NPs enhances the densification of the composite samples (Figure 4.2).

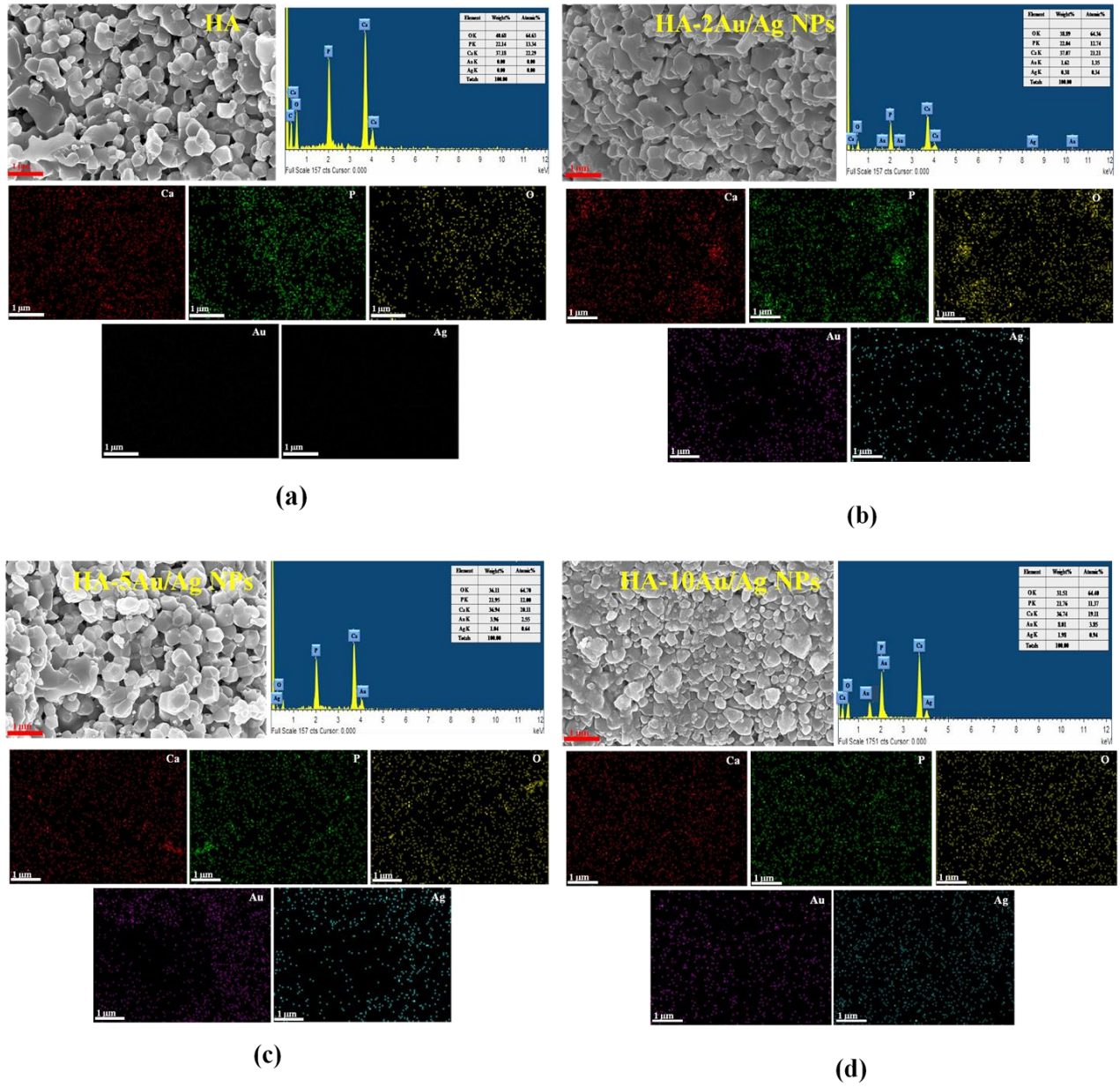

Figure 4.4 *Scanning electron micrographs, energy-dispersive X-ray spectroscopy data, and elemental mapping of fractured surfaces of a) HA, b) HA-2 Au/Ag NPs, c) HA-5 Au/Ag NPs, and d) HA-10 Au/Ag NPs sintered composites.*

EDX reveals the presence of O, P, Ca, Au, and Ag in the sintered composite samples. The result also shows an increased amount of Au and Ag with the incorporation of Au/AgNPs in HA. The elemental mapping of HA and HA-x Au/Ag NPs (x = 2, 5, and 10 wt. %) shows the uniform distribution of O, P, Ca, Au, and Ag in the sintered samples.

The XRD, SEM, EDX, and elemental mapping data indicate that there is no dissociation or diffusion of the primary elements.

4.2.3 Thermogravimetric analysis (TGA)

Figure 4.5 (a) shows the TGA curves of the functionalized Au/Ag nanoparticles. The first small amount of weight loss (~ 2 wt%, temperature up to 200°C) was attributed to the evaporation of physically adsorbed water or solvent molecules present in the sample and the second major weight loss (~18 wt%, temperature 250-450°C) was due to the decomposition of the APTMS coating.

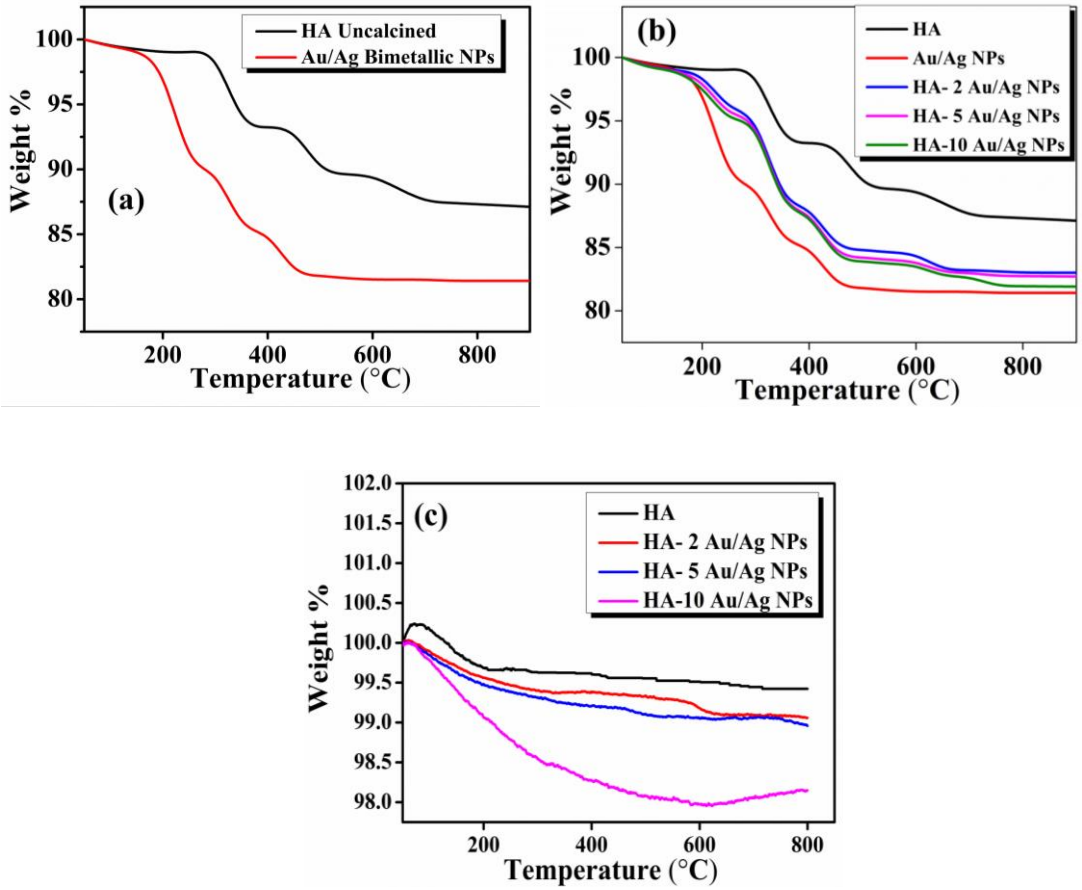

Figure 4.5 *TGA analysis of APTMS functionalized Au/Ag NPs & monolithic HA (a), HA-x Au/Ag NPs composites before sintering (b), and HA-x Au/Ag NPs composites after sintering (c).*

The TGA of the HA shown in Figure 4.5 (a) revealed the total weight loss at 50-900°C was ~ 13%. The weight loss of 0.9% occurred between 50-200°C is attributed to desorption of adsorbed water. The majority of the weight loss of ~ 12.0% occurred between 350-650° C is due to the removal of physically and chemically adsorbed water and possibly from the interstice of lattice water (Arumugam et al., 2006).

It has been reported by Furedi-Milhofer et al. 1979 that the condensation of HPO_4^{2-} group and vaporization of lattice H_2O might gradually occur at 350-650°C. Hence the condensation of HPO_4^{2-} group and evaporation of the lattice H_2O might be responsible for the weight loss in that temperature range (Sreedhar et al., 2015). The HA powder exhibited minimal weight loss in the temperature range of 650-800°C. Figure 4.5 (b and c) showed the TGA analysis of HA-x Au/Ag NPs before and after sintering. The result showed that thermal stability of Au/Ag NPs was improved when incorporated in HA matrix. Also the curve represents the decomposition temperature corresponding to both HA and APTMS functionalized Au/Ag NPs. However, the TGA curves after sintering (Figure 4.5 (c)) showed negligible weight loss.

4.2.4 Mechanical behavior

4.2.4.1 Hardness and Fracture Toughness

Indentation fracture toughness and Vickers hardness values were measured for the monolithic HA and HA-x Au/Ag NPs composite samples [Figure 4.6 (a)]. While the hardness value for monolithic HA was found to be 4.1 GPa, the hardness of the sintered HA-x Au/Ag NPs composite samples varied significantly between 5.08 and 6.87 GPa. In comparison, a hardness value of ~ 1 GPa for natural bone was reported by Zysset et al. 1999. It has been observed that incorporating Au/Ag NPs within HA increased the

hardness of the sintered samples. Whereas the monolithic HA had an indentation fracture toughness of 0.42 MPa.m$^{1/2}$, the values for the sintered composite samples ranged from 0.49 to 0.89 MPa.m$^{1/2}$. For potential load-bearing applications, the fracture toughness of this type of composite should be further strengthened. In comparison, the fracture toughness for natural bone was reported to be 2-12 MPa.m$^{1/2}$.

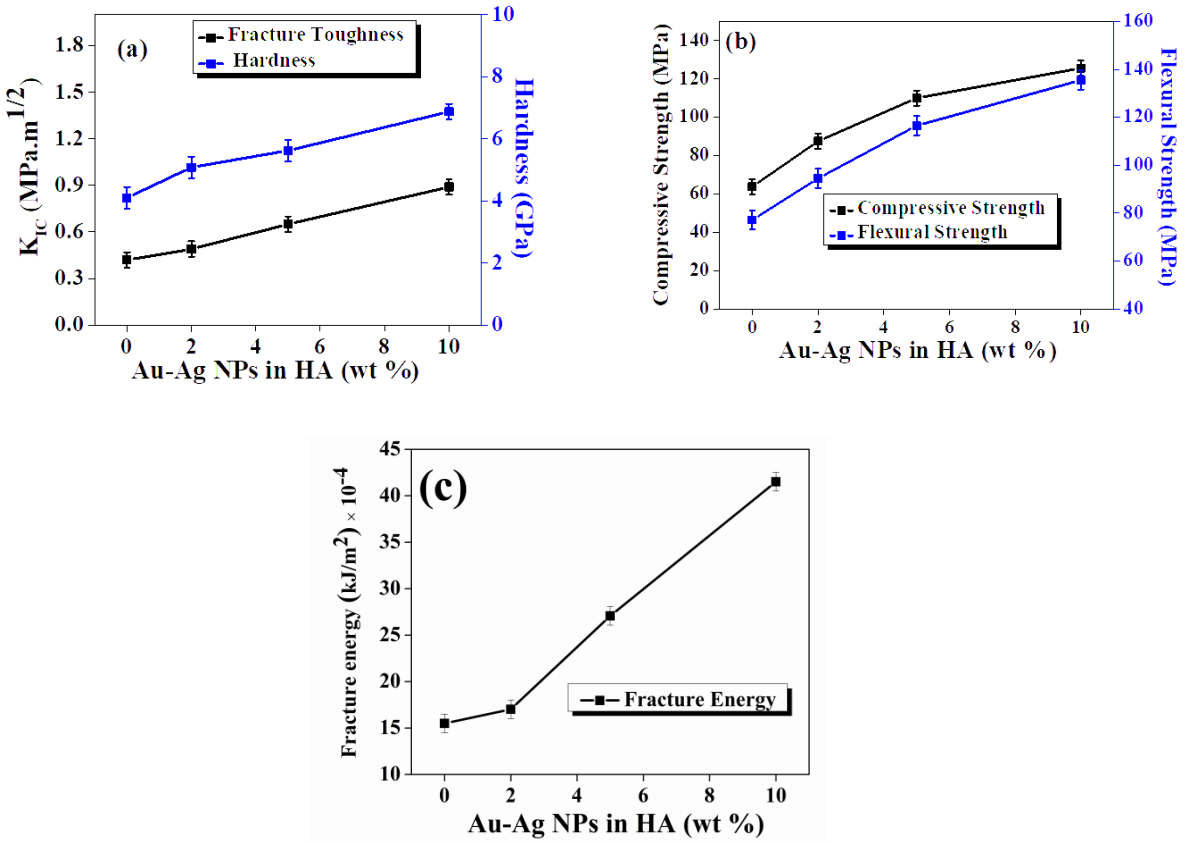

Figure 4.6 *(a) Fracture toughness and hardness and (b) compressive strength and flexural strength (c) fracture energy distribution of HA – x Au/Ag NPs (x = 0, 2, 5 and 10 wt. %) composites*

Table 4.1 shows the hardness and fracture toughness values for the monolithic HA and HA-x Au/Ag NPs composite samples. It was observed that the fracture toughness of HA was enhanced by the addition of Au/Ag nanoparticles. HA-10 Au/Ag NPs show the maximum value of fracture toughness (~ 0.89 MPa.m$^{1/2}$). It has been previously

suggested that the addition of Au/Ag nanoparticles in the matrix provides more densification after sintering, which consequently enhances the mechanical behaviour of the HA-x Au/Ag NPs composite.

4.2.4.2 Compressive and Flexural Strength

For monolithic HA and HA-x Au/Ag NPs composite systems, Table 4.1 and Figure 4.6 (b) indicate the change in compressive and flexural strength. The compressive strength of the HA-x Au/Ag NPs composite samples ranged from 87.55 to 125.62 MPa; the monolithic HA showed a lower value (63.84 MPa). It should be noted that natural bone has a compressive strength of 131 MPa along the bone axis (Reilly et al., 1974).The compressive strength of HA, which is comparable to that of natural bone, is shown to increase by approximately twice when Au/Ag NPs (10 wt. %) are incorporated into HA. After the inclusion of Au/Ag NPs in HA, the flexural strength of the sintered composites increased from 94.53 to 135.52 MPa; the monolithic HA exhibited a lower value of 77.21 MPa [Figure 4.6 (b)].

Table 4.1 *Mechanical properties of monolithic HA and HA-x Au/Ag NPs (x= 2, 5 and 10 wt. %) composite samples.*

Material	**Compressive strength (MPa)**	**Flexural strength (MPa)**	**Hardness (GPa)**	**Fracture toughness ($MPa.m^{1/2}$)**
HA	63.84	77.205	4.1	0.42
HA – 2 Au/Ag NPs	87.546	94.53	5.08	0.49
HA – 5 Au/Ag NPs	110.01	116.5	5.62	0.65
HA – 10 Au/Ag NPs	125.62	135.52	6.87	0.89

Natural cortical bone is noted to exhibit a flexural strength of approximately 160 MPa (Sedlin et al., 1965). After incorporating the Au/Ag nanoparticles in HA, the compressive strength and fracture toughness values changed, confirming the weak breakdown characteristics. The alterations in the mechanical properties of the composites may be attributed to the presence of the nanoparticles (Sahmani et al., 2019).

Figure 4.6 (c) demonstrate the calculated values of fracture energy for HA-x Au/Ag NPs (x=2, 5 and 10 wt. %) composites (Irwin et al., 1957; Sun et al., 2018). Fracture energy is a measure of the energy required to propagate a crack through a material. The fracture energy values for HA, HA- 2 Au/Ag NPs, HA- 5 Au/Ag NPs, and HA- 10 Au/Ag NPs composites have been determined to be 15.48×10^{-4} , 17.01496×10^{-4}, 27.06406×10^{-4} and 41.50742×10^{-4} kJ/m^2 , respectively. These values indicate the increasing resistance to crack propagation as the concentration of Au/Ag NPs in the HA composite increases. The incorporation of Au/Ag NPs in the HA matrix enhances the fracture energy, suggesting improved fracture toughness and resistance to crack growth. The observed trend can be attributed to the reinforcing effect of the Au/Ag NPs within the HA matrix. The presence of these nanoparticles can hinder crack propagation by acting as barriers, absorbing and dissipating energy through mechanisms such as crack deflection, particle debonding, and plastic deformation around the nanoparticles (Verma et al., 2018). Therefore, the increase in fracture energy with increasing Au/Ag NP content indicates an enhancement in the composite's ability to withstand cracking and resist fracture, making it a promising material for applications requiring improved mechanical properties and resistance to failure.

4.2.5 Bacterial Studies

4.2.5.1 MTT Assay

The variation in mean optical density (bacterial cell adhesion) for gram-positive (*S. aureus*) and gram-negative (*E. coli*) bacterial cells seeded on monolithic HA (control) and HA-x Au/Ag NPs (x=2, 5 and 10 wt. %) composite samples is shown in Figure 4.7. The incorporation of Au/Ag NPs decreases the bacterial adhesion (mean optical density) in HA. It is clearly seen by statistical analysis that the HA-x Au/Ag NPs (x=2, 5, and 10 wt. %) exhibited significant differences in mean optical density from the control sample (monolithic HA). Figure 4.7 suggested that the HA-x Au/Ag NPs (x=2, 5 and 10 wt. %) composites exhibited a statistically significant reduction in the viability of both types of bacterial cells (i.e., *S. aureus and E. coli*) with respect to the control HA.

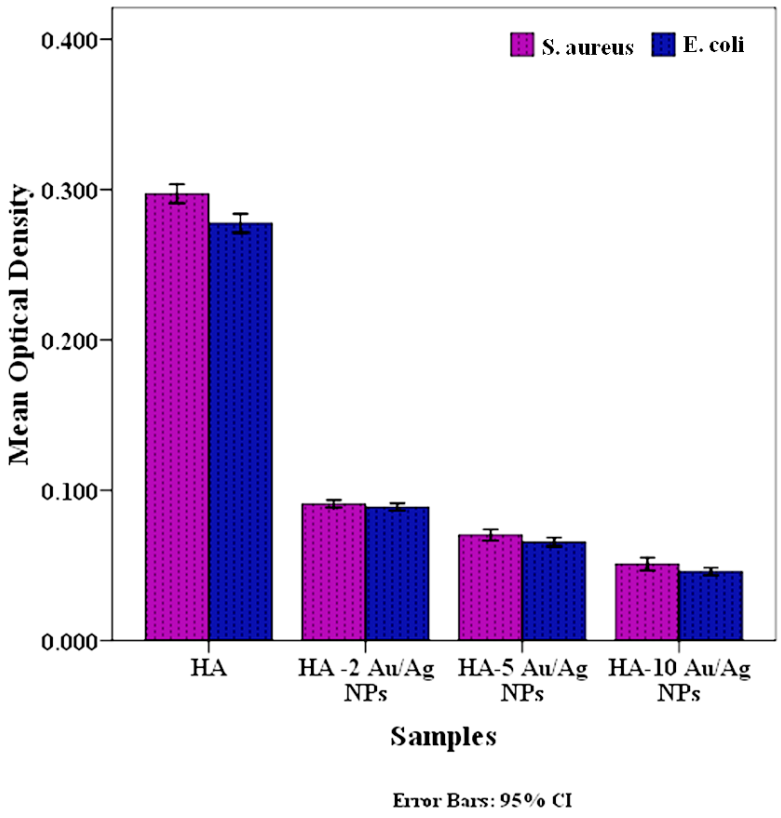

Figure 4.7 *Antibacterial response of HA, HA – 2 Au/Ag NPs, HA – 5 Au/Ag NPs, and HA – 10 Au/Ag NPs composites cultured with S. aureus and E. coli bacteria.*

When the samples were reinforced with 10% Au/Ag NPs, a significant reduction in the population of bacteria on the surface of the samples was noted. It has been reported that Ag nanoparticles exhibit greater potency toward gram-negative bacteria (Fayaz et al., 2010). Overall, the results demonstrate a significant reduction in the number of the two types of bacterial cells for the sintered HA- Au/AgNPs composite samples.

4.2.5.2 Live/Dead Assay

The live/dead assay provides qualitative analysis of the samples related to bacterial adhesion. Figure 4.8 (a) and (b) show the live and dead bacterial cells on monolithic HA and HA-x Au/Ag NPs (x=2, 5, and 10 wt. %) composite samples. It can be observed that adding Au/Ag NPs in HA reduce the population of live bacterial cells (green) compared to monolithic HA.

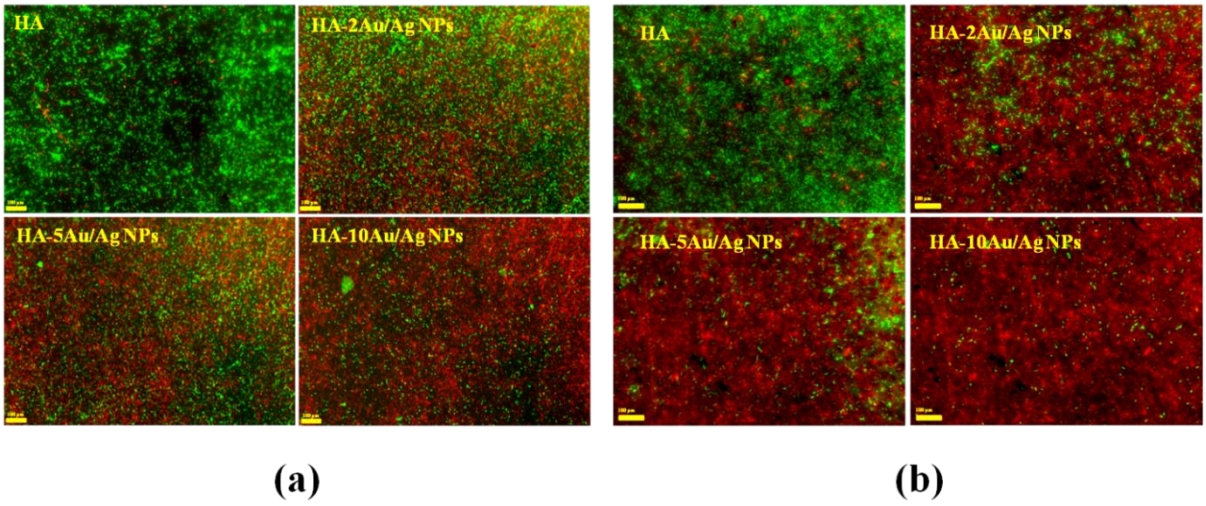

Figure 4.8 *Fluorescence microscopy images of live (green) and dead (red) S. aureus (a) and E. coli (b) bacteria cultured on HA, HA – 2 Au/Ag NPs, HA – 5 Au/Ag NPs and HA – 10 Au/Ag NPs composites.*

In addition, the HA-x Au/Ag NPs exhibited a greater population of dead bacterial (e.g., *S. aureus* and *E. coli*) cells. Overall, this qualitative study result corroborates the quantitative study result for the HA and HA-x Au/Ag NPscomposite samples.

4.2.5.3 Super Oxide Radical (SOD) Assay

Superoxide production by *S. aureus* (gram-positive) and *E. coli* (gram-negative) cells cultured on sintered HA and HA-x Au/Ag NPs composites is shown in Figure 4.9 (a). It is clearly observed that there are significantly more SOD production withHA-x Au/Ag NPs composites as compared to monolithic HA for both types of bacterial cells (Figure 4.9 (a)). In addition, it was found that despite the difference in the two types of bacteria, the variation in concentration of the Au/Ag NPs secondary phase escalates the superoxide production in cultured composite samples. Previous studies suggest that the production of ROS directly indicates antibacterial behavior (Tan et al., 2016; Ong et al., 2017).

The Fenton reaction can explain this kind of antimicrobial behavior. It proposes that the superoxide destabilizes ferrous (Fe^{2+}) ions by disrupting iron-sulfur clusters in proteins that are present in bacterial cells, which interact with hydrogen peroxide to produce hydroxyl radicals (Fenton reaction: $Fe^{2+} + H_2O_2 \rightarrow Fe^{3+} + HO^{\bullet} + OH$) (Blanc et al., 2015; Verma et al., 2020). These free radicals cause oxidative stress, which disrupts the bacterial cell membrane (Blanc et al., 2015; Verma et al., 2020).

4.2.5.4 Lipid peroxidation (LPO) Assay

The calculated MDA equivalent for HA and HA-x Au/Ag NPs composite samples cultured with *S. aureus* and *E. coli* cells is shown in Figure 4.9 (b). This Figure indicates that incorporating Au/Ag NPs as the secondary phase enhances the MDA level of HA for

S. aureus and *E. coli* cells. The oxidative damage appears to be caused by polyunsaturated lipids as described by the LPO mechanism. MDA, which is assessed as a measure of LPO, is created when the polyunsaturated fatty acids disintegrate under oxidative stress (Verma et al., 2020; Grotto et al., 2009). MDA forms an adduct with TBA that exhibits an optimum value of absorbance at 532 nm, which consequently shows greater MDA formation and produces more LPO. As a result, bacterial cells are damaged.

4.2.5.5 Catalase Activity Assay

Figure 4.9 (c) shows the catalase activity in a quantitative manner. Catalase is an anti-oxidant enzyme that dissolves hydrogen peroxide into water and oxygen, preserving the cells from oxidative damage (Verma et al., 2020; Hadwan et al., 2018). In this study, the catalase activity is measured in terms of spectrophotometric measurement of H_2O_2 hydrolysis. The absorbance value obtained from this measurement exhibits the amount of H_2O_2 (substrate) remaining in the reaction mixture, which is inversely proportional to catalase activity. It is clearly observed that the graph shows a continuous decrease in the absorbance value with the addition of Au/Ag NPs as the secondary phase in HA.

Figure 4.9 (c) shows that regardless of the bacteria type tested, the maximum decomposition of $H_2O_2$was obtained for HA-10 Au/Ag NPs, which indicates the optimum antibacterial behavior.

4.2.5.6 Protein Estimation

Protein estimation is used to evaluate the total protein present. The basic principle of this methodology is that proteins react with alkaline cupric sulfate to form a tetradentate cuprous complex in the presence of sodium potassium tartrate. This Cu^{+} present in the

cuprous complex then reduces Folin's reagent to a deep blue color solution, which is monitored spectrophotometrically at 750nm (Schaich et al., 2016).

Protein + Cu^{2+} ⟶ tetradentate cuprous complex ⟶ reduced Folin's reagent

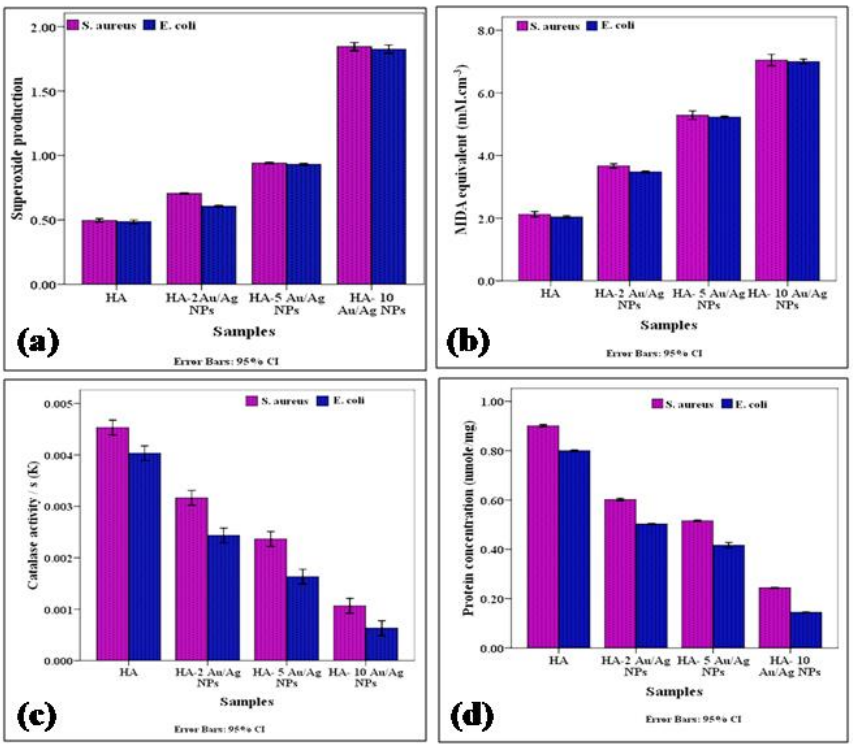

Figure 4.9 *(a) Superoxide production (ROS generation), (b) lipid peroxidation in terms of MDA equivalent, (c) catalase activity, (d) protein estimation of HA, HA – 2 Au/Ag NPs, HA – 5 Au/Ag NPs, and HA – 10 Au/Ag NPs composites cultured with S. aureus and E. coli bacteria.*

Figure 4.9 (d) shows that the addition of Au/Ag NPs in HA decreases the value of protein present. The lowest amount of protein was noted for HA – 10 Au/Ag NPs. As reported earlier, oxidative stress results in DNA damage, cell wall damage, and protein degradation; the results of the SOD, LPO, and catalase assays support this result.

It has been suggested that the generation of reactive oxygen species (ROS) such as hydroxyl ions, peroxides, and superoxides on the composite surface is another factor that affects the antibacterial response due to their toxicity towards bacterial cells (Murphy et al., 2011; Chen et al., 2011).

Figure 4.10 depicts a schematic illustration of how Ag particles inhibit bacterial development. Ag particles first break down into Ag^+ and are then drawn to the negatively charged surface of the bacteria. Ag^+ ions interact with the bacterial membrane and enter the bacteria through transmembrane proteins (Solioz et al., 1995.These Ag^+ damage DNA, denaturing the DNA molecules (Klueh et al., 2000). Additionally, Ag^+ attaches to the thiol (-SH) groups in the enzymes, forming strong S-Ag bonds that eventually render the enzymes inactive.

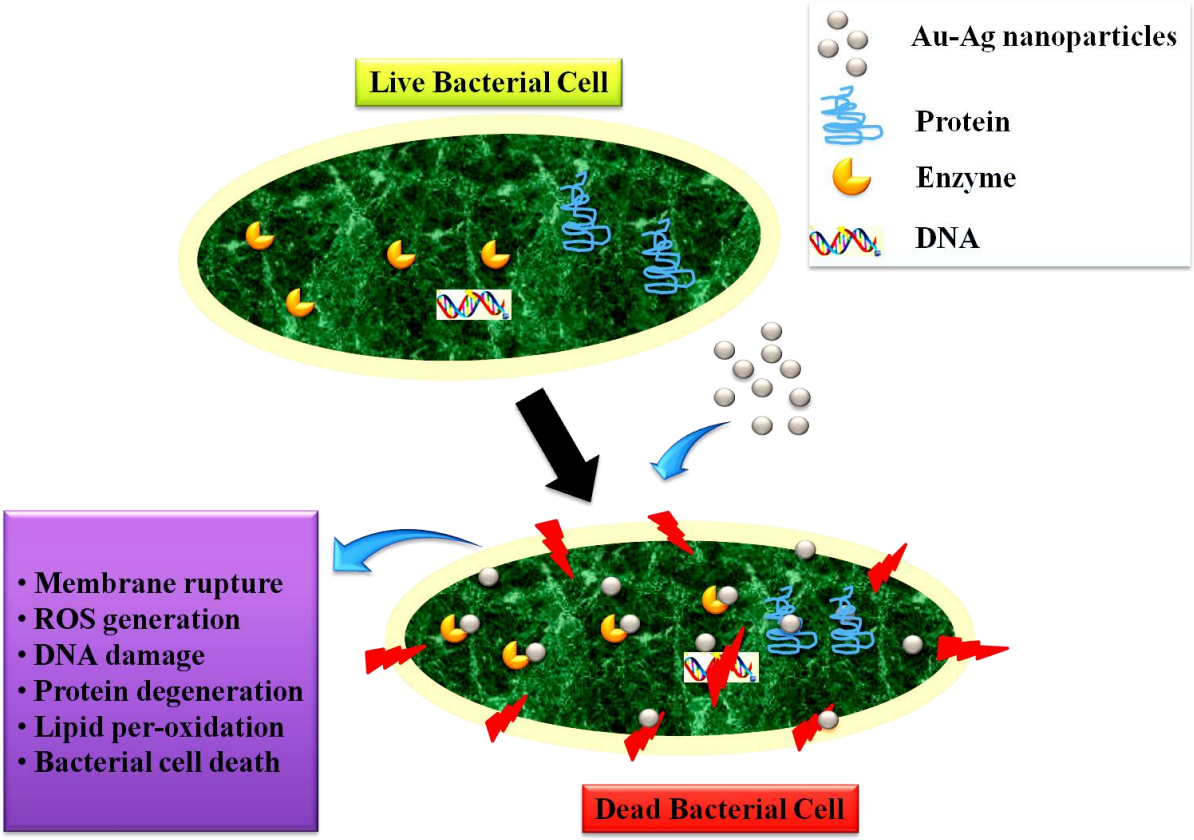

Figure 4.10 *Schematic diagram for antibacterial response due to the presence of Ag NPs in HA- Au/Ag NPs composite samples.*

Additionally, Ag catalyzes oxidation events that produce disulfide bonds (R-S-S-R). The shape and functionality of the enzymes are influenced by the formation of disulfide linkages (Davies et al., 1997). In addition, Ag release kinetics in the solution plays a significant part in determining the antibacterial activity. According to Song et al., Ag produced plasmolysis, or the separation of a bacterial cytoplasm from its cell wall (Song et al., 2006). Egger et al. postulated that the peptidoglycans present in bacterial cell walls contain teichoic acids or lipoteichoic acids with a significant negative charge that may interact with free Ag^+ ions (Egger et al., 2009). Rannie and Barggs (Barggs et al., 1974) demonstrated that silver ions might interact with DNA bases as well as sulfydryl (-SH) groups of proteins, resulting in the inhibition of respiratory mechanisms. This study demonstrated how the addition of Au/Ag NPs as the secondary phase enhances the multifunctional properties of HA.

4.2.6 Eukaryotic Cell Studies

4.2.6.1 Cell Viability

Figure 4.11 shows the MTT assay result for MG-63 cells cultured on control HA and HA-x Au/Ag NPs after 3, 5, and 7 days of incubation in terms of mean optical density (OD). The variation in the value of mean OD reflects cell proliferation with respect to the incubation period. A significant difference in cell proliferation was observed for 5- and 7-day cultured cells in comparison to cells incubated for 3 days, irrespective of sample type. In addition, within the same incubation period, it was found that the cell proliferation rate was higher for HA-10Au/Ag NPs in comparison to pure HA and other composite samples.

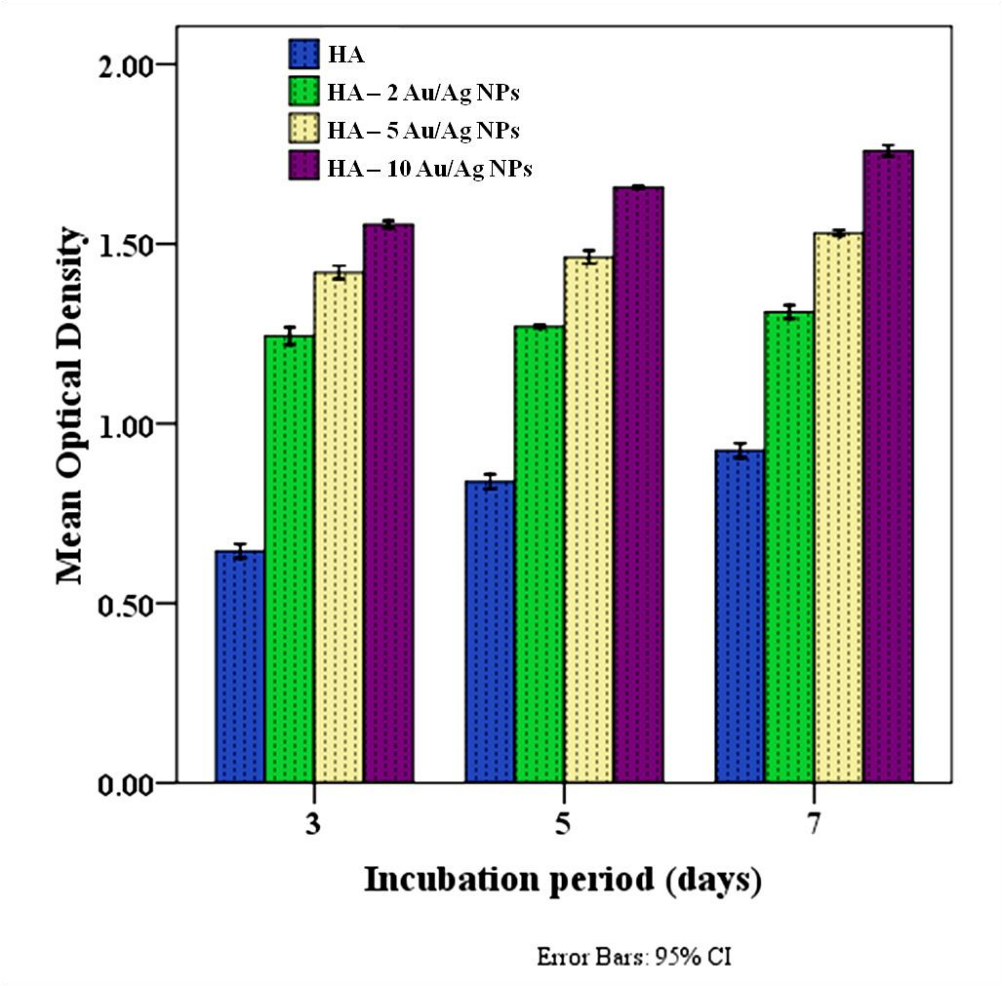

Figure 4.11 *Cytocompatibility of HA, HA – 2 Au/Ag NPs, HA – 5 Au/Ag NPs, and HA – 10 Au/Ag NPs composites cultured with MG-63 cells.*

4.2.6.2 Cell Morphology Studies

Figure 4.12 shows the fluorescence images of MG-63 cells cultured on different samples. It was clearly observed that the cell density was higher on HA-x Au/Ag NPs surfaces than on the HA control. In addition, the cells seem to be more flattened, indicating better cell adhesion.

On the other hand, the osteogenic potential of Ag and Au nanoparticles has been reported previously. Qing et al. reported that Ag nanoparticles enhance osteogenesis by upregulating different BMPs (Qing et al., 2018). Another study reported that Au

nanoparticles enhance osteogenesis through the extracellular signal-regulated kinases/mitogen-activated protein kinases signaling pathway (Liu et al., 2010).

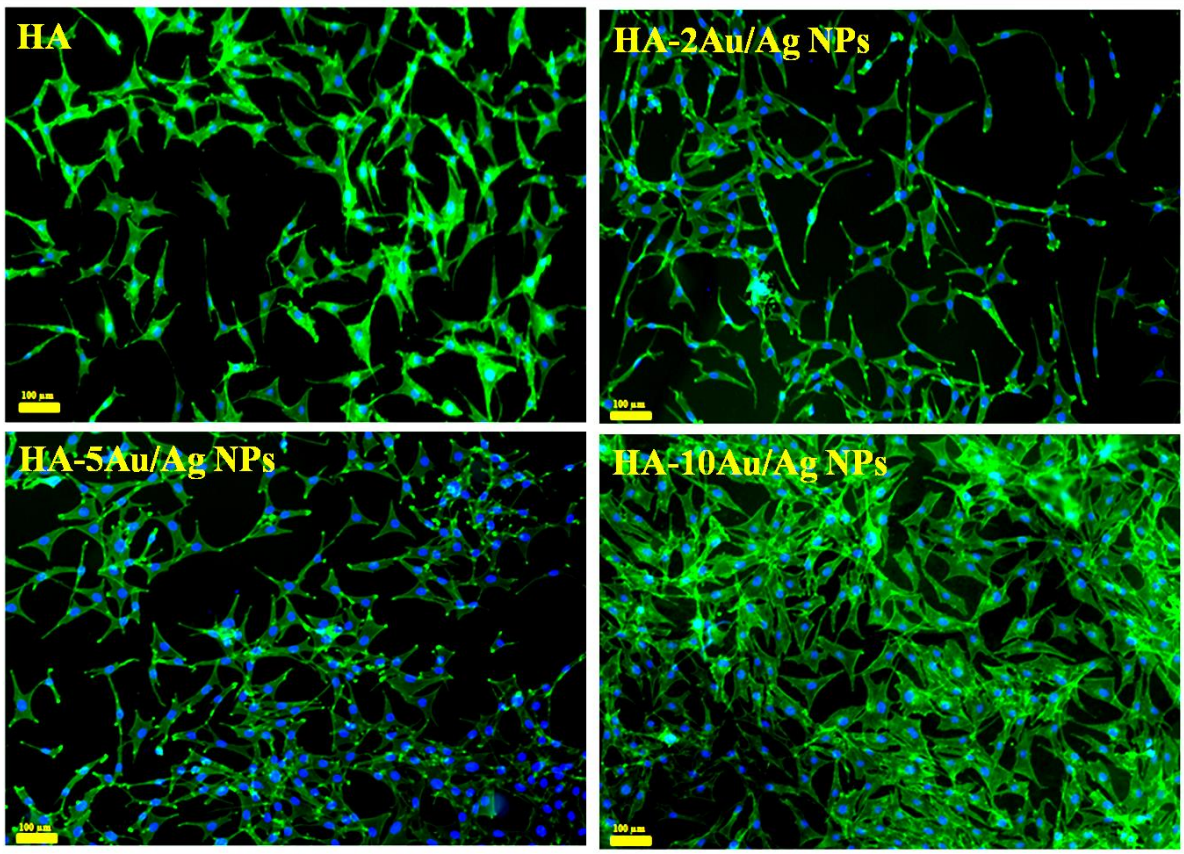

Figure 4.12 *Qualitative cellular response (fluorescence images), representing the morphology of MG-63 cultured on (a) HA, (b) HA – 2 Au/Ag NPs, (c) HA – 5 Au/Ag NPs, and (d) HA – 10 Au/Ag NPs composites.*

This finding can possibly explain how Ag and Au may play an essential role in bone regeneration and formation alongside HA. Gold nanoparticles (AuNPs) have been extensively studied in a scope of biomedical applications, including cancer treatment, drug delivery, gene delivery, cell tracking, biosensing, and regenerative medicine (Emami et al., 2015; Karimi Zarchi et al., 2018). AuNPs have outstanding qualities that include high surface area-to-volume ratio values, biocompatibility, chemical inertness, chemical stability, and processing via straightforward synthesis approaches. AuNPs are

known to enhance bone cell differentiation and proliferation as well as serve as an osteogenic agent (Ribeiro et al., 2017; Heo et al., 2014; Zhang et al., 2021; Samadian et al., 2021). By stimulating the p38 mitogen-activated protein kinase (MAPK) pathway, AuNPs induce osteoinductive activity in mesenchymal stem cells (MSCs) (Yi et al., 2010). In addition, recent results indicate the potential of AuNPs as osteoinductive biomaterials for bone tissue engineering and regeneration (Bala et al., 2006; Yi et al., 2010). It was reported that AuNPs caused human bone marrow-derived mesenchymal stem cells to differentiate into osteoblasts (hMSCs). HA-Au nanoparticles demonstrated good cytocompatibility and were taken up by hMSCs. The enhanced osteogenic differentiation of hMSCs was demonstrated by the high levels of ALP production, calcium mineralization, and the expression of conventional osteogenic genes (Liang et al., 2019; Zhang et al., 2021; Ge et al., 2018). Furthermore, the incorporation of Au appeared to involve the osteoinductive potential of HA-Au nanoparticles, involving the activation of the Wnt/-catenin signaling pathway.

Based on the existing knowledge and our findings, an appealing hypothesis is that Ag and Au when combined with HA may have an additive effect by jointly enhancing bone regeneration and formation. These investigations suggest that the strategy of combined Ag, Au, and HA treatment may be an effective therapeutic approach for bone regeneration and repair.

4.3 Conclusion

The main objective of this study was to develop a HA-based biocomposite with enhanced mechanical, antibacterial, and cellular functionality. The addition of Au/Ag NPs to HA significantly improved the mechanical properties; HA – 10Au/Ag NPs exhibited the optimum mechanical among the composite samples. The antibacterial behavior against

gram positive (*S. aureus*) and gram negative (*E. coli*) bacteria of HA was augmented by the incorporation of Au/Ag NPs. It was demonstrated quantitatively and qualitatively that the viability of gram-positive (*S. aureus*) and gram-negative (*E. coli*) bacteria on composite surfaces was significantly diminished due to mechanisms such as the bactericidal characteristics of Ag NPs and ROS generation. In addition, quantitative and qualitative analyses reveal the enhanced cytocompatibility of HA and the HA-x Au/Ag NPs composite due to the incorporation of Au/Ag NPs. In summary, the inclusion of Au/Ag NPs improves the mechanical properties, antibacterial behavior, and *in vitro* biocompatibility of HA.